Abnormal Strain Rate Sensitivity Driven by a Unit Dislocation-Obstacle Interaction in bcc Fe

Zhitong Bai and Yue Fan

Abnormal strain rate sensitivity driven by a unit dislocation-obstacle interaction in BCC Fe

Zhitong Bai, Yue Fan[*]

Department of Mechanical Engineering, University of Michigan, Ann Arbor, Michigan, 48109, USA

Abstract

The interaction between an edge dislocation and a sessile vacancy cluster in bcc Fe is investigated over a wide range of strain rates from $10^8 s^{-1}$ down to $10^3 s^{-1}$, which is enabled by employing an energy landscape-based atomistic modeling algorithm. It is observed that, at low strain rates regime less than $10^5 s^{-1}$, such interaction leads to a surprising negative strain rate sensitivity behavior because of the different intermediate microstructures emerged under the complex interplays between thermal activation and applied strain rate. Implications of our findings regarding the previously established global diffusion model are also discussed.

[*]Corresponding author: fanyue@umich.edu

Advanced reactors are being designed for longer lifetimes while operating in extreme conditions of temperature and irradiation [1]. The neutron-irradiated ferritic alloys typically include super-saturated defects such as self-interstitial atom and vacancy clusters [2]. The interactions between such defect clusters and dislocations are critical to understand and predict the mechanical degradations of the materials, such as swelling, creep, and embrittlement [3-5].

Negative strain-rate sensitivity (nSRS) is a remarkable phenomenon showing an inverse relation between flow stresses and applied strain rates [6-8], which might lead to detrimental effects such as non-uniform deformation and mechanical instabilities [9]. It is challenging to explain nSRS by the direct interaction between a dislocation and an obstacle. Because according to the classical picture [10], the activation barrier for a local dislocation-obstacle interaction monotonically decreases as stress increases. Two direct implications stem from this picture: (i) the qualitative interaction mechanism is presumably unaffected by surrounding environments; and (ii) only a positive correlation between strain rate and flow stress, can be obtained by employing the kinetics theory. Therefore, to explain the nSRS phenomenon, a global diffusion scheme has been proposed: there is an adequate supply of defects that diffuse towards the dislocation, and lower strain rate allows more time for defects concentrate at dislocation core, which yields a stronger resistance and a higher flow stress [9]. Several continuum models have been developed to quantify the nSRS behavior. For example, by assuming the obstacle and dislocation concentrations are time and strain dependent, Estrin *et al.'s* model can predict an inverse behavior if the homogenous nucleation of obstacles in bulk being taken place [11,12]. Curtin *et al's* pioneering work has provided the supporting evidence to such global diffusion scheme from the fundamental level by investigating the mechanism of direct single-atomic jump across the dislocation slip plane [13]. In the present work, instead of focusing on global diffusions and concentrations of solutes, we probe a local interaction between a dislocation and a sessile obstacle over a wide range of strain rates, from $10^8 s^{-1}$ down to $10^3 s^{-1}$. We show that the critical resolved shear stress (CRSS) is determined by the complex interplay between thermal activation and applied strain rate. Because of different intermediate microstructures emerged at various strain rate conditions, a non-monotonic variation of CRSS and a nSRS at low strain rates have been observed. Such newly identified

mechanism, together with the established global diffusion scheme, might enable a more comprehensive understanding towards the evolutions of irradiated microstructure.

Vacancy clusters or voids are common defects in structural materials and can induce strong resistance to the glide motion of edge dislocation [14]. In this paper, we therefore consider the interaction between the $1/2<111>$ edge dislocation and a small void containing 9 vacancies in bcc Fe. The simulation system has the dimensions $9.81nm$ (x) $*3.51nm$ (y)$*12.57nm$ (z), and contains 33171 atoms. Periodic boundary conditions are applied on the dislocation line and glide directions, respectively. An embedded atom method (EAM) type potential [15] is employed. Atomistic modeling on dislocation-obstacle interactions at low strain rate (less than 10^6s^{-1}) has been known as a challenge to molecular dynamics (MD) simulations [14]. Recently, a potential energy landscape (PEL)-based modeling framework combining the autonomous basin climbing (ABC) method and transition state theory (TST) has been proposed [16,17], which makes it possible to probe considerably lower strain rate conditions than in regular MD simulations. A schematic illustration of the modeling framework is shown in Fig.1. At a given strain condition (including the initial state at zero strain), employ ABC to obtain the local dominant reaction pathway and associated activation barrier E_b in the system's underlying PEL. The corresponding thermal activation time at a given temperature can be calculated as $\Delta t = [v_0 e^{-E_b/k_B T}]^{-1}$, according to the TST, where v_0 is the attempt frequency around $10^{13}s^{-1}$ [18]. For a specified strain rate $\dot{\varepsilon}$, the calculated strain increment, $\Delta \varepsilon = \dot{\varepsilon}\Delta t = \dot{\varepsilon}[v_0 e^{-E_b/k_B T}]^{-1}$, is then applied to the system. Keep doing the procedures iteratively until the dislocation is unpinned from the obstacle, one can then investigate the microstructural evolutions and associated stress-strain curves at prescribed strain rate and temperature.

To be more specific, a few atom layers near the top and the bottom (green regions) are set as rigid blocks in the simulation cell. The shear strain is implemented into the system by displacing the upper block as a whole [19]. At each strain state, the total force along the dislocation glide direction on the upper block, F_b, is calculated. The shear stress is then calculated as F_b/S_t, where S_t is top surface area of the upper block. The CRSS is regarded as

the peak stress of the stress-strain curve. More details of the model, in what we now call ABC-T, can be found in [16,17].
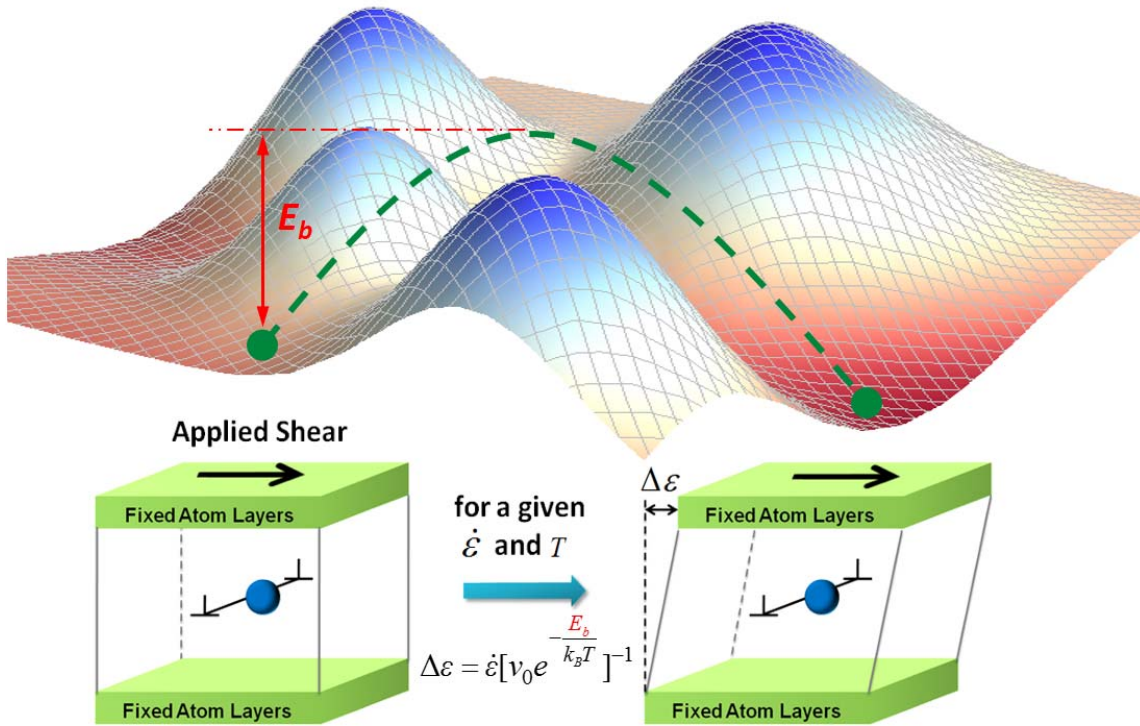

Fig.1. Illustration for the dynamic model in capturing the dislocation-obstacle interaction as a function of strain rate, $\dot{\varepsilon}$, and temperature, T, after combing the autonomous basin climbing (ABC) method and transition state theory (TST).

We first studied the interaction between the dislocation and the vacancy cluster under static conditions. Fig. 2 shows the strain-stress curve, associated potential energy (per atom on average), and corresponding critical configurations.

(a)
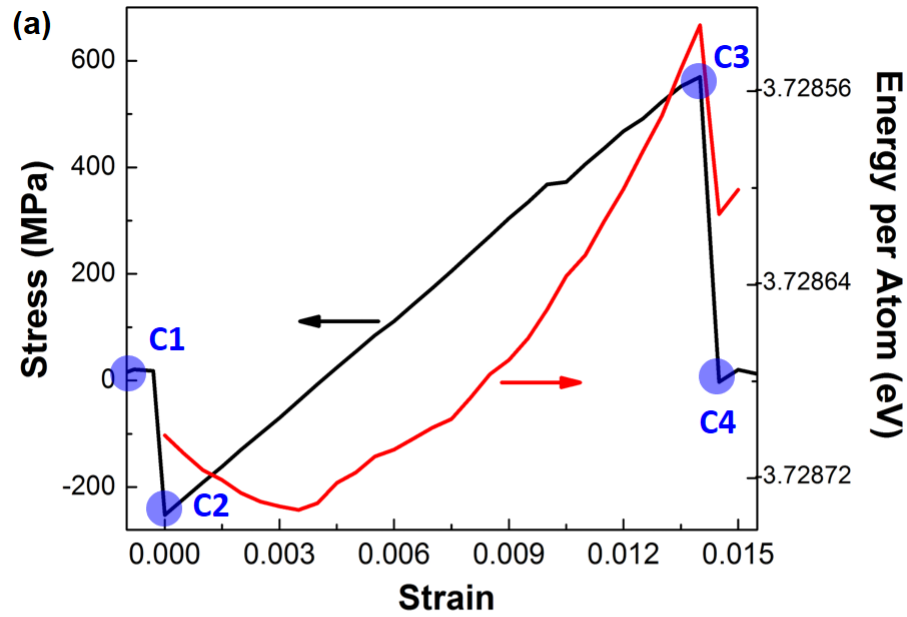
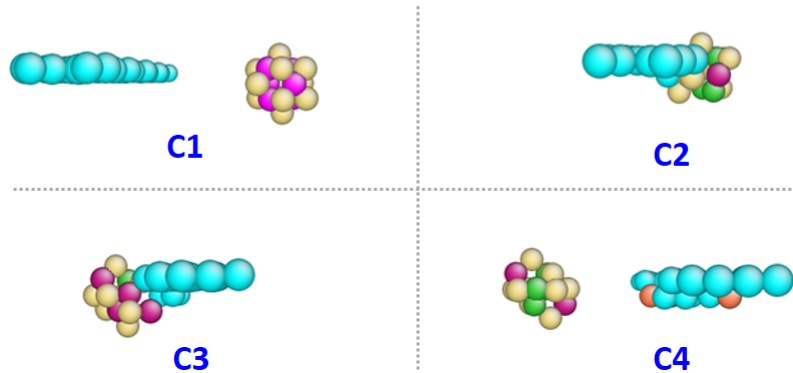**(b) Critical Configurations**

C1

C2

C3

C4

Fig.2: (a) The strain-stress curve, and associated potential energy (per atom on average) of the system, during the static interaction. (b) Critical atomistic configurations during the static interaction as shown in (a). The atoms are visualized by Atomeye [20], and colored according to different coordinate numbers.

In the beginning, the vacancy cluster is on the right side of the dislocation, with the center of mass placed on the glide plane. Upon shear loading, the dislocation is attached to the vacancy cluster (Fig.2(b), C2) associated with a stress relaxation down to -251 MPa, indicating a very strong attractive pinning interaction in the early stage [19]. To better mimic the strain-controlled tensile test experimental condition, it is convenient to study the interaction as a function of strain. The corresponding strain at C2 is therefore set to be zero as a reference state. By further increasing the strain, there is a monotonic increase of the stress

from C2 to C3. When the stress increases up to 570 MPa, the dislocation and vacancy cluster are detached from each other, leading to the sharp stress relaxation. The corresponding potential energy of the system during the interaction is also shown by the red curve in Fig.2(a). Two vacancies in the void are absorbed by the dislocation during the static interaction, and a small jog is formed after the interaction (Fig.2(b), C4).

We then probe the same interaction at room temperature and five different strain rates from 10^8 s^{-1} down to 10^3 s^{-1}, by employing ABC-T. The results are benchmarked against independent MD simulations at the high strain rates (10^6 s^{-1} and 10^8 s^{-1}), where MD is known to be valid. Fig.3(a-b) show the corresponding strain-stress curves provided by ABC-T and MD simulation, respectively. It can be seen that all the CRSS at non-zero temperature are lower than the critical stress found in static calculation. It is also noticed that in the MD simulations (seen in Fig.3(b)), the stress at the beginning is around -170 MPa, which is 80 MPa deviated from the static results (black curve in Fig.3(a)). We believe such discrepancy is mainly attributed to the thermal compression stress produced in MD simulations, because of the fixed volume control (see Supplemental Materials [21]). The atomistic configurations after the interactions are shown in Fig. 3(c). Compared to 2 vacancies being absorbed in static condition, 5 vacancies are absorbed by the dislocation under 300 K, while different strain rates lead to different atomic configurations after the interactions. In ABC-T results, a most compact structure of vacancy cluster is formed under $10^3 s^{-1}$, as seen in Fig.3(c). The remaining vacancy clusters for the strain rates between $10^4 s^{-1}$ and $10^8 s^{-1}$ are in the same structure, while the jogged dislocation at $10^8 s^{-1}$ has a relatively ripped structure because of the extremely high strain rate. As seen in Fig.3(c), independent MD simulations show identical vacancy cluster configurations as in ABC-T results under the same conditions. The slight differences in dislocation structures are due to the atom oscillations in non-zero temperature MD simulations.
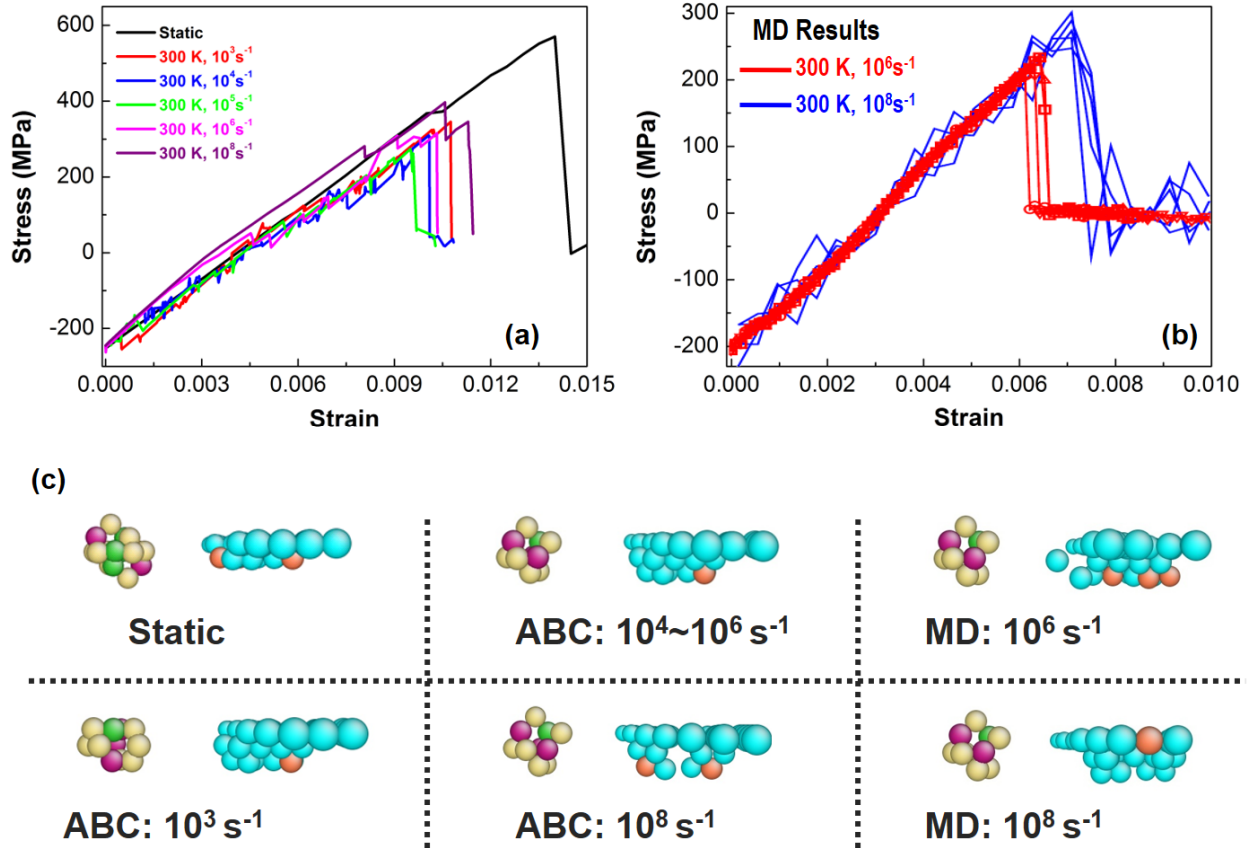
Fig.3 (a-b) The stress-strain curves for the dislocation void interaction under different strain rate conditions, provided by ABC-T and MD simulations, respectively. (c) The associated critical atomic configurations after the interaction.

The CRSS under different strain rates are read off from Fig.3(a-b) and plotted in Fig.4. According to ABC-T results, for strain rates higher than $10^5 s^{-1}$ the CRSS increases as a function of strain rate, which shows a normal relation and is consistent with earlier studies [24,25]. It is noticed that under the same conditions, there are quantitative mismatches of CRSS between ABC-T and MD. The reasons could be twofold: (i) It might again originate from the thermal compression stress in MD simulations mentioned above; (ii) The attempt jump frequency v_0 in ABC-T is set as $10^{13} s^{-1}$. Although such value has been widely used and accepted, it might become larger upon strong entropy effects [26], which could lead to a

7

More importantly, in spite of the quantitative mismatch, if one focuses on the net increases of CRSS from $10^6 s^{-1}$ to $10^8 s^{-1}$, then clearly both ABC-T and MD studies show the same results. The agreements on the CRSS variations, along with the identical configurations shown in Fig.3(c), demonstrate the robustness of ABC-T algorithm in probing the dislocation-obstacle interactions.
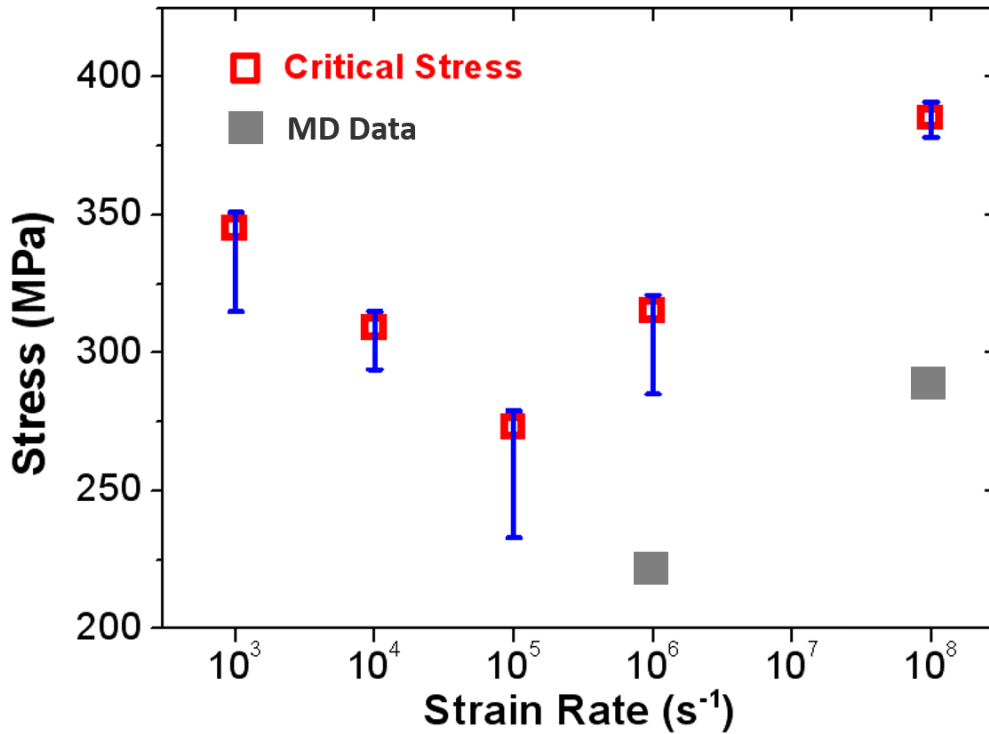

Fig.4. The CRSS under different strain rates conditions. Red open squares are the results of ABC-T framework simulations, while the black squares represent the MD simulations results.

Very interestingly, and surprisingly, the CRSS shows a nSRS behavior below $10^5 s^{-1}$ in ABC-T. To reveal the underpinnings of such phenomenon, we focus on the potential energy changes of the system during the evolutions, following the similar ideas proposed by Dutta *et al* [27] and Monnet [28]. For each set of strain rate, a parabola like shape of the potential energy is observed, similarly as the red curve in Fig.2(a). Fig.5(a) shows the energy differences at various strain rate conditions, with respect to the static interaction energy (red curve in Fig.2(a)). As seen in the figure, at relatively low strain rate $10^4 s^{-1}$, there are more

frequent fluctuations on the energy difference curve, indicating significant amount of thermal activations and relaxations. For the higher stain rates such as $10^6 s^{-1}$, the energy difference curve is smoother, which demonstrates the system is mainly driven by strain. It is worth noting that a similar serrate-smooth transition has also been observed in nano-indentation experiments, by increasing the applied strain rates [29].
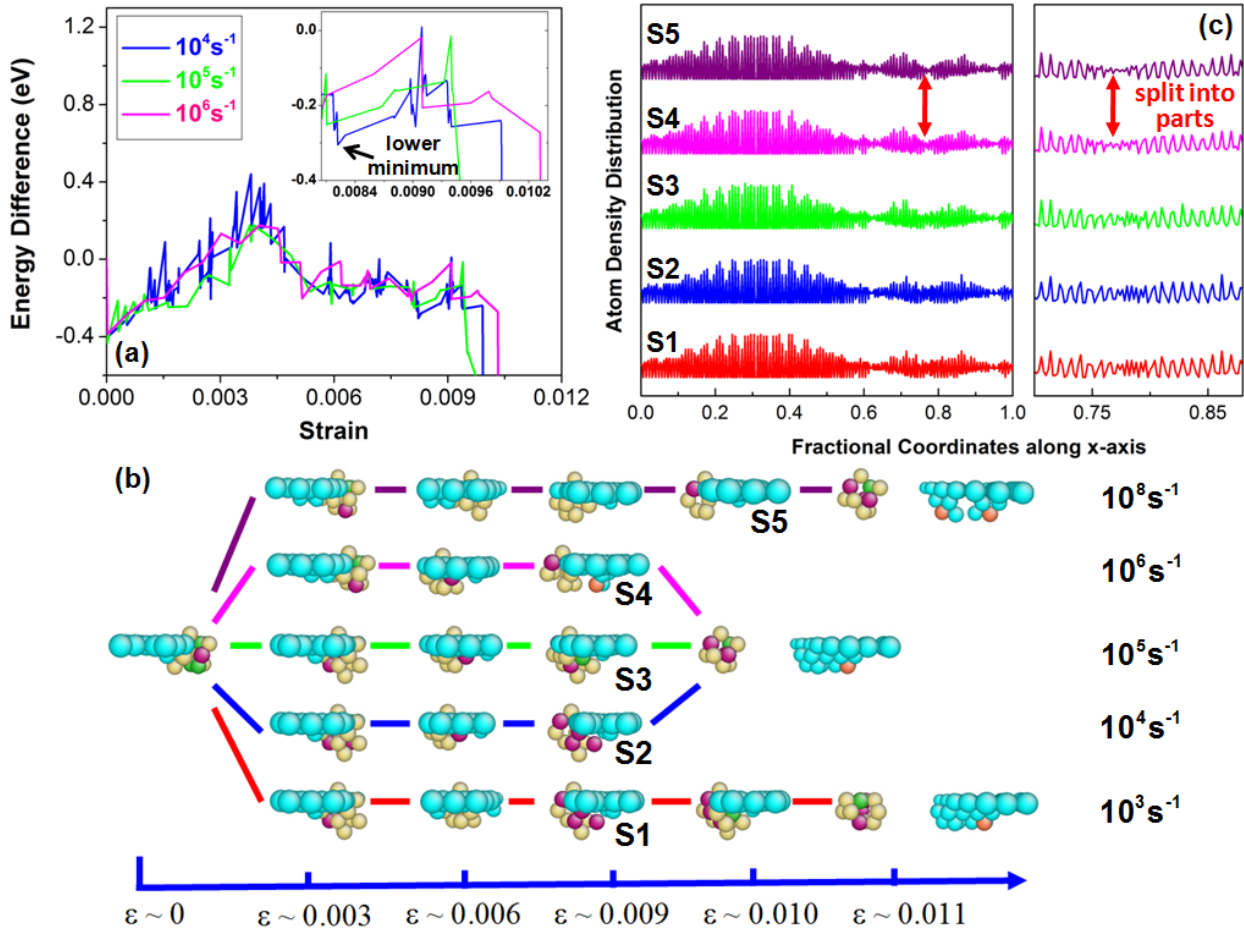

Fig.5. (a) The potential energy differences of the system under different strain rates conditions, with respect to the static energy curve. (b) The atomistic configurations during the interactions, at various strain rates. (c) The atom density distributions along x-axis, *i.e.* the <111> direction, for structures S1-S5. The vacancy cluster's fractional coordinate along x-axis is about 0.8. It clearly shows that for high strain rates $10^6 s^{-1}$ and $10^8 s^{-1}$, the vacancy clusters are ripped into parts, while such behavior is not observed for lower strain rates.

The defect structure evolutions under different strain rates are shown in Fig.5(b). At early strain stage ($\varepsilon \sim 0.003$), the vacancy cluster is nucleated downward due to the thermal activation, for those strain rates between $10^3 s^{-1}$ and $10^5 s^{-1}$. However, under high strain rates of

9

10^6s^{-1} and 10^8s^{-1}, no such nucleation is observed because there is not enough time for this event to be thermally activated.

Assisted by thermal activations, the dislocation core glides to the right side of vacancy cluster at medium strain stage (seen in Fig.5(b), the configurations at ε~0.006 for the strain rate between 10^3s^{-1} and 10^6s^{-1}). This process is associated with the energy peak between ε=0.003 and ε=0.006 shown in Fig.5(a). On the other hand, for the highest strain rate 10^8s^{-1}, the dislocation does not glide to the right side of the vacancy cluster until the strain reaches the level around 0.009. This is because, at very high strain rate condition, the thermal activations are significantly suppressed and the similar interaction mechanism can only take place at deferred strain [16,30].

Upon further deformation, the structures of vacancy cluster show different evolutions at various conditions, as seen from S1-S5 in Fig.5(b). Under the strain rates between 10^3s^{-1} and 10^5s^{-1}, the vacancy clusters show downward nucleation due to thermal activations (S1-S3 in Fig.5(b)). However, at 10^6s^{-1} and 10^8s^{-1}, the vacancy cluster is being ripped into parts (see S4 and S5 in Fig.5(b)) rather than being nucleated, because there is not enough time for this event to be thermally activated at very high strain rates. The atomic density projection [19] along x-axis (gliding direction of dislocation) shown in Fig.5(c) also demonstrates a clear split behavior at high strain rates. It is worth noting that, there are still strong connections between the ripped parts because their spatial spans are comparable with the cut-off radius of the EAM potential. Therefore, effectively the ripped structure at high strain rate imposes a larger surface area attaching to the dislocation core. At lower strain rate between 10^3s^{-1} and 10^5s^{-1}, the vacancy clusters nucleate to different structures (S1-S3). S1 and S2 are in a relatively looser structure than S3, and the lower energy minimum in the inset plot of Fig.5(a) indicates that they are energetically more stable than S3. For both the loose structure (S1-S2) and the ripped structure (S4-S5), they have larger surface areas attached to the dislocations than S3 does. Correspondingly, the larger areas induce stronger impedances, and thus lead to higher critical stresses. This explains the reason that the CRSS reaches its minimum at 10^5s^{-1}.

By comparing the further evolutions between 10^3s^{-1} and 10^4s^{-1}, it can be found that the loose structure of vacancy cluster under 10^3s^{-1} (S1) further nucleates to another stable configuration, because of more available time for thermal activation under lower strain rate.

Subsequently, the stable structure leads to a higher CRSS than that in $10^4 s^{-1}$. Therefore, in the entire simulated strain rate regime from $10^3 s^{-1}$ to $10^8 s^{-1}$, the CRSS shows a "V" shape as seen in Fig.4.

It is worth noting that the minimum strain rate considered here is $10^3 s^{-1}$. In principle ABC-T method would allow to tackle even slower processes. However, as illustrated in Fig.1, at a given temperature too small strain rate can only implement a negligible strain increment during each iteration, which will tremendously increase the total computational costs. As a comparison, typical experiments concerning the dislocation-obstacle interactions are usually done in the strain rate regime between $10^0 s^{-1}$ and $10^{-3} s^{-1}$ [31-33], which seems still slower than the present study by several orders of magnitude. But we would like to note that, such low rates usually refer to the global strain rates applied to the entire specimens in the *mm* order. And experiments [34,35] show that the deformation in the specimen is highly heterogeneous and largely localized within the so-called dislocation channels, of which the width is in the order of tens of *nm*. In other words, inside those channels where dislocation-obstacle interactions take place, the local strain rates can be up to 10^5 (~1*mm*/ 10*nm*) times larger than the average global strain rates. Since the present study focuses on the local dislocation-obstacle interaction, we therefore believe the hereby obtained results are not unrealistic.

In summary, we have examined a dislocation-vacancy cluster interaction in bcc Fe by a recently developed framework, ABC-T, which allows to extend the atomistic modeling to low strain rate conditions. We demonstrate the dislocation-obstacle interaction is determined by two competitive factors: strain rate and thermal activation. Under low strain rates, thermal activations assist the vacancy cluster in nucleating to more stable states (S1 and S2 in Fig.5(b)), which induces a stronger resistance to the dislocation and therefore lead to a higher CRSS than that in $10^5 s^{-1}$. However, under high strain rates such as $10^6 s^{-1}$ and $10^8 s^{-1}$, there is not enough time for the vacancy cluster nucleation being thermally activated. In contrast, the vacancy cluster is ripped to parts (S4 and S5 in Fig.5(b)) due to the high strain rate. These parts impose a larger total area attached to the dislocation than the compact structure in $10^5 s^{-1}$ (S3 in Fig.5(b)), which also leads to a stronger interaction with the dislocation and thus higher

CRSS. All these together explain the underlying mechanism for the "V"-shape relation between CRSS and strain rate, with the minimum at $10^5 s^{-1}$.

The inverse relation between CRSS and strain rate is known as the nSRS phenomenon, which could induce detrimental effects on the materials, such as the decreased ductility and strength, and the onset of mechanical instabilities [9,13]. Understanding and explaining such behavior are therefore critical for the material design strategies. In this work, we particularly examine the strain rate effects on the local interaction between a dislocation and a sessile obstacle. Through direct atomistic simulation we demonstrate that, in addition to the previously proposed global diffusion models [11-13], the local dislocation-obstacle interaction can also lead to the nSRS behavior.

We would like to stress that although the present study focuses on the non-monotonic variation of CRSS in a BCC Fe system, the underlying principle—namely the complex interplay between thermal activation and mechanical loading—is rather general and applicable to many different materials. For example, it has been found in a large variety of materials (including Al, Cu, Ni, Zr, and intermetallic γ-TiAl) [16,17,36] that the microstructural evolutions of dislocations can be qualitatively different at different timescales. And the transitions between various mechanisms have been viewed as an underlying competition of strain rate and thermal activation, corroborating the spirit of the present study. As a final note, in addition to the strain rate effects probed in the present study, there are many other factors (e.g. system size, type of obstacle, *etc*) could also affect the microstructural evolutions, which would warrant further studies in the future.

References

[1]   R. W. Grimes, R. J. Konings, and L. Edwards, Nature Materials **7**, 683 (2008).
[2]   V. Shastry and T. D. de la Rubia, Journal of Engineering Materials and Technology **121**, 126 (1999).
[3]   L. K. Mansur, Journal of Nuclear Materials **216**, 97 (1994).
[4]   G. S. Was, Journal of Nuclear Materials **367-370**, 11 (2007).
[5]   G. R. Odette, M. J. Alinger, and B. D. Wirth, Annual Review of Materials Research **38**, 471 (2008).
[6]   A. Kipelova, R. Kaibyshev, V. Skorobogatykh, and I. Schenkova, Journal of Physics: Conference Series **240**, 012100 (2010).
[7]   M. A. Lebyodkin, Y. Brechet, Y. Estrin, and L. P. Kubin, Physical Review Letters **74**, 4758 (1995).
[8]   A. Bertram, T. Böhlke, C. Brüggemann, Y. Estrin, and M. Lebyodkin, PAMM **6**, 353 (2006).
[9]   J. M. Robinson and M. P. Shaw, International Materials Reviews **39**, 113 (1994).
[10]   U. F. Kocks, A. S. Argon, and M. F. Ashby, in *Progress in Materails Science*, edited by B. Chalmers, J. W. Christian, and T. B. Massalski (Pergamon Press, New York, 1975), p. 110.
[11]   Y. Brechet and Y. Estrin, Acta Metallurgica Et Materialia **43**, 955 (1995).
[12]   S. Zhang, P. G. McCormick, and Y. Estrin, Acta Materialia **49**, 1087 (2001).
[13]   W. A. Curtin, D. L. Olmsted, and L. G. Hector, Nature Materials **5**, 875 (2006).
[14]   D. J. Bacon, Y. N. Osetsky, and D. Rodney, in *Dislocations in Solids*, edited by J. P. Hirth, and L. Kubin (Elsevier, 2009), pp. 1.
[15]   G. J. Ackland, D. J. Bacon, A. F. Calder, and T. Harry, Philosophical Magazine A **75**, 713 (1997).
[16]   Y. Fan, Y. N. Osetskiy, S. Yip, and B. Yildiz, Proceedings of the National Academy of Sciences **110**, 17756 (2013).
[17]   X. Yan and P. Sharma, Nano Letters **16**, 3487 (2016).
[18]   A. F. Voter, in *Radiation Effects in Solids* edited by K. E. Sickafus, E. A. Kotomin, and B. P. Uberuaga (Springer, Berlin, 2007), p. 1~24.
[19]   D. J. Bacon, Y. N. Osetsky, and D. Rodney, in *Dislocations in Solids*, edited by J. P. Hirth, and L. Kubin (Elsevier, 2009), pp. 1.
[20]   L. Ju, Modelling and Simulation in Materials Science and Engineering **11**, 173 (2003).
[21]   See Supplemental Material [url] for the discrepancy between the ABC-T and MD method due to the thermal compression stress, which includes Refs. [16, 22,23].
[22]   S. Alexander, Modelling and Simulation in Materials Science and Engineering **18**, 015012 (2010).
[23]   C. L. Kelchner, S. J. Plimpton, and J. C. Hamilton, Phys. Rev. B **58**, 11085 (1998).
[24]   D. Terentyev, L. Malerba, D. J. Bacon, and N. O. Yu, Journal of Physics: Condensed Matter **19**, 456211 (2007).
[25]   D. Terentyev, Y. N. Osetsky, and D. J. Bacon, Scripta Materialia **62**, 697 (2010).
[26]   B. P. Uberuaga, R. G. Hoagland, A. F. Voter, and S. M. Valone, Physical Review Letters **99**, 135501 (2007).
[27]   A. Dutta, M. Bhattacharya, N. Gayathri, G. C. Das, and P. Barat, Acta Materialia **60**, 3789 (2012).
[28]   G. Monnet, Acta Materialia **55**, 5081 (2007).
[29]   C. A. Schuh and T. G. Nieh, Journal of Materials Research **19**, 46 (2004).
[30]   Y. Fan, Y. N. Osetsky, S. Yip, and B. Yildiz, Physical Review Letters **109**, 135503 (2012).
[31]   F. Onimus and J.-L. Béchade, Journal of Nuclear Materials **384**, 163 (2009).

[32]   F. Onimus, I. Monnet, J. L. Béchade, C. Prioul, and P. Pilvin, Journal of Nuclear Materials **328**, 165 (2004).

[33]   J. W. Dunlop, Y. J. M. Bréchet, L. Legras, and Y. Estrin, Materials Science and Engineering: A **443**, 77 (2007).

[34]   K. Farrell, T. S. Byun, and N. Hashimoto, Journal of Nuclear Materials **335**, 471 (2004).

[35]   N. Hashimoto, T. S. Byun, K. Farrell, and S. J. Zinkle, Journal of Nuclear Materials **329-333**, 947 (2004).

[36]   H. Wang, D. S. Xu, D. Rodney, P. Veyssière, and R. Yang, Modelling and Simulation in Materials Science and Engineering **21**, 025002 (2013).